Inorganic Chemistry

Article

pubs.acs.org/IC

From Antiferromagnetic to Ferromagnetic Interaction in Cyanido-Bridged Fe(III)–Ru(II)–Fe(III) Complexes by Change of the Central Diamagnetic Cyanido-Metal Geometry

Xiao Ma,[†] Sheng-Min Hu,[†] Chun-Hong Tan,[†] Yong-Fan Zhang,*[,‡,§] Xu-Dong Zhang,[†] Tian-Lu Sheng,*[,†] and Xin-Tao Wu[†]

[†]State Key Laboratory of Structural Chemistry, Fujian Institute of Research on the Structure of Matter, Chinese Academy of Science, Fuzhou, Fujian 350002, P. R. China

[‡]Department of Chemistry, Fuzhou University, Fuzhou, Fujian 350108, P. R. China

[§]Fujian Provincial Key Laboratory of Theoretical and Computational Chemistry, Xiamen, Fujian 361005, P. R. China

Supporting Information

ABSTRACT: *Cis*- and *trans*-isomeric heterotrinuclear-metallic complexes and their two-electron-oxidation products, *cis*-/*trans*-[Cp(dppe)Fe(μ-CN)Ru(bpy)$_2$(μ-CN)Fe(dppe)Cp][PF$_6$]$_2$ (*cis*-/*trans*-**1**[PF$_6$]$_2$) and *cis*-/*trans*-[Cp(dppe)Fe(μ-CN)Ru(bpy)$_2$(μ-CN)Fe(dppe)Cp][PF$_6$]$_4$ (*cis*-/*trans*-**1**[PF$_6$]$_4$), have been synthesized and structurally characterized. To the best of our knowledge, the complexes are the first example of a *cis*-/*trans*-isomer with multistates. Although separated by the diamagnetic cyanido-metal bridge, the two distant paramagnetic metal centers in both the oxidized complexes exhibit quite strong magnetic couplings. As a unique example, *cis*-**1**[PF$_6$]$_4$ is antiferromagnetic, and *trans*-**1**[PF$_6$]$_4$ is ferromagnetic. Density functional theory (DFT) calculations suggest that the spin-delocalization mechanism should be responsible for the magnetic interactions between the two distant paramagnetic Fe(III) centers across the diamagnetic cyanido-metal in both *cis*- and *trans*-**1**$^{4+}$. Most importantly, the DFT calculations revealed that the type (antiferromagnetic or ferromagnetic) and strength (J) of the magnetic interactions in such compounds can be controlled by the variation (*cis* or *trans*) of the diamagnetic central metal configurations.

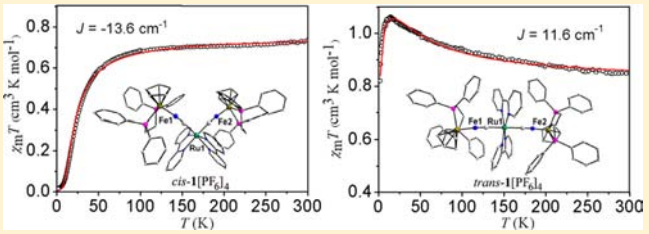

INTRODUCTION

The study of the magnetic properties of cyanido-bridged compounds has recently attracted great interest from the viewpoint of practical applications and for basic science.[1−3] In the past two decades, much effort in this field has been devoted to the study of the cyanido-bridged compounds in which the paramagnetic metal ions are directly bridged by the CN$^-$ ions.[2] As is well-known, the classic cyanido-bridged compound, Fe$^{III}_4$[Fe^{II}(CN)$_6$]$_3$·xH$_2$O (Prussian blue), in which the paramagnetic Fe(III) ions are bridged by the diamagnetic Fe(II) ions,[4] shows ferromagnetic ordering.[5] However, the magnetic chemistry of those polynuclear compounds with a diamagnetic cyanidometal separating two magnetic centers has rarely been studied,[6] mainly because magnetic coupling between two paramagnetic metal centers rapidly weakens and even disappears as the distance between the metal centers increases.[3,7] Therefore, the preparation of such compounds with a strong magnetic coupling is still a great challenge in this field. We are interested in the investigation of polynuclear compounds with a bridging diamagnetic cyanidometal ligand,[6I] because it is possible to control the magnetic properties of such compounds by more strategies such as a change of the configuration or the ligands of the central bridging cyanidometal. In this work, diamagnetic Ru^{II}(bpy)$_2$(CN)$_2$ was selected as such a bridging cyanidometal ligand. In order to investigate whether magnetic coupling between the distant metal centers can be controlled by the geometry of the central bridging cyanidometal ligand, both diamagnetic *cis*- and *trans*-Ru^{II}(bpy)$_2$(CN)$_2$ were used as starting materials. Herein, we describe the syntheses, crystal structures, and magnetic properties of *cis*- and *trans*-[Cp(dppe)Fe^{III}(μ-CN)Ru(bpy)$_2$(μ-CN)Fe^{III}(dppe)Cp][PF$_6$]$_4$ (*cis*-**1**[PF$_6$]$_4$ and *trans*-**1**[PF$_6$]$_4$; dppe = 1,2-bis(diphenyl-phosphino)ethane; bpy = 2,2′-bipyridine). Density functional theory (DFT) calculations were performed to explore the mechanism of the long-distance magnetic interactions in these complexes and the influence on magnetic coupling by the *cis* or *trans* configuration of the central bridging cyanidometal ligand.

RESULTS AND DISCUSSION

Synthesis and Characterization. The reaction of *cis*- and *trans*-Ru(bpy)$_2$(CN)$_2$ with two equivalents of Cp(dppe)Fe(NCCH$_3$)Br in methanol yielded complexes *cis*- and *trans*-**1**[PF$_6$]$_2$. The cyclic voltammograms of *cis*- and *trans*-**1**[PF$_6$]$_2$ were measured respectively in acetonitrile. As shown in Figure

Received: June 27, 2013
Published: September 16, 2013

   dx.doi.org/10.1021/ic401604q | Inorg. Chem. 2013, 52, 11343−11350

1 and Figure S1, the cyclic voltammograms of *cis*- and *trans*-**1**$[PF_6]_2$ show two reversible redox processes, indicating that

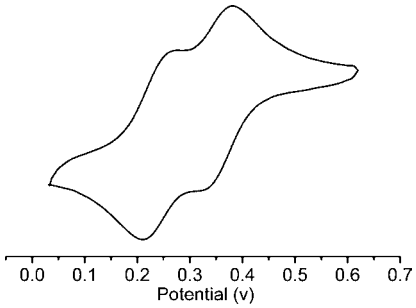

Figure 1. Cyclic voltammogram of complex *cis*-**1**$[PF_6]_4$ in a 0.10 M acetonitrile solution of Bu_4NPF_6 at a scan rate of 100 mV s^{-1}.

there exist metal−metal interactions of two external Fe^{II} atoms in *cis*/*trans*-**1**$[PF_6]_2$. It should be noted that the oxidation potentials of *trans*-**1**$[PF_6]_2$ ($E_{1/2}$(**1**) = 0.26 V, $E_{1/2}$(**2**) = 0.37 V) are slightly more positive than the corresponding ones of *cis*-**1**$[PF_6]_2$ ($E_{1/2}$(**1**) = 0.25 V, $E_{1/2}$(**2**) = 0.36 V), suggesting that the *cis*-form is easier to be oxidized than the *trans*-form. On the basis of the electrochemistry measurements, their oxidation by two equivalents of $(Cp)_2FePF_6$ produced *cis*- and *trans*-**1**$[PF_6]_4$. All four complexes have been fully characterized by elemental analysis, MS-ESI, ^{31}P NMR, UV−vis−NIR, and IR (see the Experimental Section and the Supporting Information). The IR spectra of the four complexes exhibited different C≡N stretching frequencies (Supporting Information, Figures S2−S3). From complexes *cis*- and *trans*-**1**$[PF_6]_2$ (2086 cm^{-1} for *cis*-**1**$[PF_6]_2$, 2099 cm^{-1} for *trans*-**1**$[PF_6]_2$) to the oxidized complexes (2059 and 2021 cm^{-1} for *cis*-**1**$[PF_6]_4$, 2041 cm^{-1} for *trans*-**1**$[PF_6]_4$), the ν(CN) band is shifted to a lower frequency, suggesting that the energy of the ν(CN) stretch decreases with the oxidation state of the cyanido-nitrogen coordinated metal. The similar phenomenon has also been previously observed[8] and recently analyzed by DFT calculations.[9]

Single Crystal X-Ray Structure Analysis. The molecular structures of all four complexes were determined by single crystal X-ray analysis (Supporting Information, Figures S4−S7; Table 1). Selected bond lengths for *cis*- and *trans*-**1**$[PF_6]_4$ are listed in Figure 2. As shown in Figure 2, the two terminal Cp(dppe)Fe fragments are bridged by the central Ru-$(bpy)_2(CN)_2$ units in the *cis*- and *trans*-configurations with C−Ru−C bond angles of 95.4(1) and 179.3(3)°. By comparison of *cis*/*trans*-$\mathbf{1}^{4+}$ with *cis*/*trans*-$\mathbf{1}^{2+}$, it can be seen that the Ru^{II}−C_{CN} bond lengths in *cis*/*trans*-$\mathbf{1}^{4+}$ (av. *cis* = 1.962 Å, *trans* = 2.015 Å) are slightly shorter than those in *cis*/*trans*-$\mathbf{1}^{2+}$ (av. *cis* = 1.991 Å, *trans* = 2.058 Å). Meanwhile, the Fe−N bond lengths in *cis*/*trans*-$\mathbf{1}^{4+}$ (av. *cis* = 1.897 Å, *trans* = 1.891 Å) are significantly shorter than those in *cis*/*trans*-$\mathbf{1}^{2+}$ (av. *cis* = 1.930 Å, *trans* = 1.936 Å). In contrast, the Fe^{III}−P bond lengths in *cis*/*trans*-$\mathbf{1}^{4+}$ (av. *cis* = 2.269 Å, *trans* = 2.258 Å) are longer than those of Fe^{II}−P in *cis*/*trans*-$\mathbf{1}^{2+}$ (av. *cis* = 2.204 Å, *trans* = 2.211 Å).

UV−Vis−NIR Absorption Spectroscopy. The UV/vis/NIR spectra of *cis*/*trans*-$\mathbf{1}^{4+}$ and *cis*/*trans*-$\mathbf{1}^{2+}$ in CH_3CN are shown in Figure 3. From the figure, it can be found that complexes *cis*/*trans*-$\mathbf{1}^{2+}$ do not exhibit any absorption band in the NIR region, but their two-electron-oxidation products *cis*/*trans*-$\mathbf{1}^{4+}$ display a relatively intense NIR band at a λ_{max} of 722 nm for *cis*-$\mathbf{1}^{4+}$ and 783 nm for *trans*-$\mathbf{1}^{4+}$, respectively. The two NIR bands are attributed to the Ru(II)→Fe(III) metal to metal charge transfer (MMCT).[10] The red-shift of about 61 nm of *trans*-$\mathbf{1}^{4+}$ relative to *cis*-$\mathbf{1}^{4+}$ shows that the former has a lower MMCT energy. According to the Hush formalism,[11] it can be

Table 1. Crystallographic Data for *cis*-1$[PF_6]_2$, *cis*-1$[PF_6]_4$, *trans*-1$[PF_6]_2$, and *trans*-1$[PF_6]_4$

	cis-**1**$[PF_6]_2$	*cis*-**1**$[PF_6]_4$	*trans*-**1**$[PF_6]_2$	*trans*-**1**$[PF_6]_4$
formula	$RuFe_2C_{88}H_{88}N_6O_3P_6F_{12}$	$RuFe_2C_{84}H_{80}N_6O_3P_8F_{24}$	$RuFe_2C_{84}H_{74}N_6P_6F_{12}$	$RuFe_2C_{92}H_{90}N_{10}O_2P_8F_{24}$
fw (g/mol)	1904.23	2138.07	1794.08	2284.27
T (K)	293	293	293	293
crystal system	monoclinic	monoclinic	monoclinic	orthorhombic
space group	$P2_1/c$	$P2_1/c$	$C2/c$	$C222_1$
Z	4	4	4	4
a [Å]	11.550	17.145	19.325	13.166
b [Å]	34.840	20.734	15.251	30.941
c [Å]	25.912	29.012	27.224	24.979
α [deg]	90.00	90.00	90.00	90.00
β [deg]	110.650	97.440	94.316	90.00
γ [deg]	90.00	90.00	90.00	90.00
V [$Å^3$]	9757	10226.7	8001	10175.4
density (calcd.) [$g{\cdot}cm^{-3}$]	1.296	1.389	1.489	1.491
μ [mm^{-1}]	0.614	0.640	0.741	0.649
θ range [deg]	2.05−25.50	2.50−27.48	2.22−25.00	2.10−27.50
reflns collected	59703	76243	24765	38200
unique reflns	17921	23249	6915	11591
obsd reflns ($I > 2\sigma(I)$)	12274	18961	5102	9750
params refined	1145	1207	479	631
final R indices (obsd reflns)[a]	0.0783	0.0609	0.0860	0.0769
final R indices (all reflns)[a]	0.1106	0.0748	0.1140	0.0875
GOF (goodness of fit)	1.053	1.068	1.059	1.034

[a] $R_1 = \sum(||F_o| - |F_c||)/\sum|F_o|$. $wR_2 = [\sum w(|F_o^2| - |F_c^2|)^2/\sum w|F_o^2|^2]^{1/2}$.

dx.doi.org/10.1021/ic401604q | *Inorg. Chem.* 2013, 52, 11343−11350

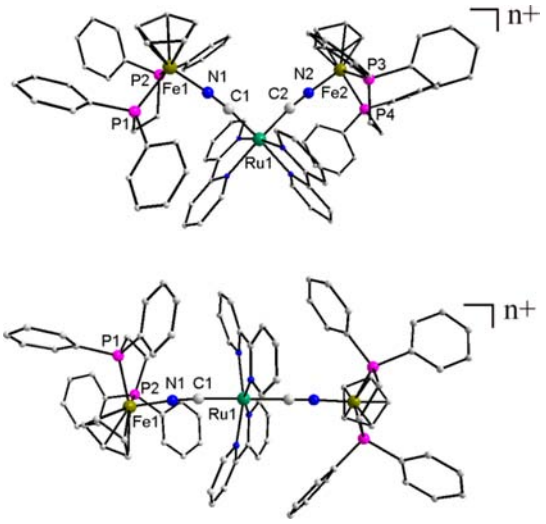

Figure 2. Molecular structures of *cis*-$\mathbf{1}^{n+}$ (n = 2, 4; top) and *trans*-$\mathbf{1}^{n+}$ (n = 2, 4; bottom; counterions, solvent molecules, hydrogen atoms were omitted for clarity). Selected bond lengths (Å): Ru1−C1 1.991(5), Ru1−C2 1.990(6), Fe1−N1 1.942(5), Fe2−N2 1.918(5), Fe1−P 2.199 (av), Fe2−P 2.209 (av), in *cis*-$\mathbf{1}^{2+}$. Ru1−C1 1.959(3), Ru1−C2 1.964(3), Fe1−N1 1.901(3), Fe2−N2 1.892(3), Fe1−P 2.266 (av), Fe2−P 2.271 (av) in *cis*-$\mathbf{1}^{4+}$. Ru1−C1 2.058(7), Fe1−N1 1.936(6), Fe1−P 2.211 (av) in *trans*-$\mathbf{1}^{2+}$. Ru1−C1 2.015(5), Fe1−N1 1.891(4), Fe1−P 2.258 (av) in *trans*-$\mathbf{1}^{4+}$.

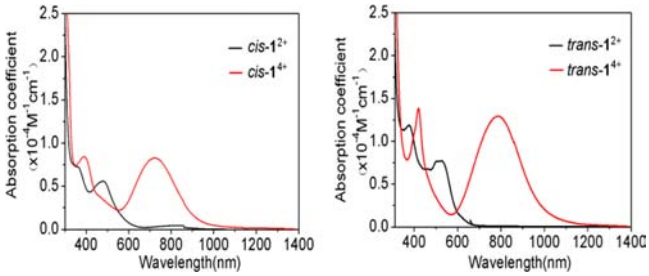

Figure 3. UV/vis/NIR spectra of *cis*-$\mathbf{1}^{2+}$ (black trace) and *cis*-$\mathbf{1}^{4+}$ (red trace) in CH_3CN (left). UV/vis/NIR spectra of *trans*-$\mathbf{1}^{2+}$ (black trace) and *trans*-$\mathbf{1}^{4+}$ (red trace) in CH_3CN (right).

calculated that the delocalization parameters α^2 are 0.0208 for *cis*-$\mathbf{1}^{4+}$ and 0.0332 for *trans*-$\mathbf{1}^{4+}$, respectively. This suggests that the electron delocalization between Ru(II) and Fe(III) in *trans*-$\mathbf{1}^{4+}$ is stronger than in *cis*-$\mathbf{1}^{4+}$.

Mössbauer Spectra. To gain insight into the spin state of complexes *cis*/*trans*-$\mathbf{1}^{4+}$ from room to low temperature, ^{57}Fe Mössbauer spectra were recorded at 298 and 40 K. The quadrupole splitting (QS) and isomer shift (IS) parameters are given in Table 2. The spectra of *cis*-$\mathbf{1}^{4+}$ at 40 and 298 K are shown in Figure 4. As shown in Figure 4, for *cis*-$\mathbf{1}^{4+}$ only one doublet was observed at both 40 and 298 K. The parameters of IS = 0.338 mm/s and QS = 0.698 mm/s at 40 K and of IS = 0.264 mm/s and QS = 0.705 mm/s at 298 K are typical of low-spin Fe(III).[12] The Mössbauer spectra of *trans*-$\mathbf{1}^{4+}$ at 40 and 298 K show that the Fe(III) atoms in the complex are also low-spin (Supporting Information, Figures S8 and S9). These finds are consistent with the magnetic measurement results of both the complexes (see below).

Table 2. ^{57}Fe Mössbauer Fitting Parameters for *cis*-$\mathbf{1}^{4+}$ and *trans*-$\mathbf{1}^{4+}$ at 40 and 298 K

compound	IS (mm/s)	QS (mm/s)
cis-$\mathbf{1}[PF_6]_4$ (40 K)	0.338	0.698
cis-$\mathbf{1}[PF_6]_4$ (298 K)	0.264	0.705
trans-$\mathbf{1}[PF_6]_4$ (40 K)	0.443	1.121
trans-$\mathbf{1}[PF_6]_4$ (298 K)	0.258	0.779

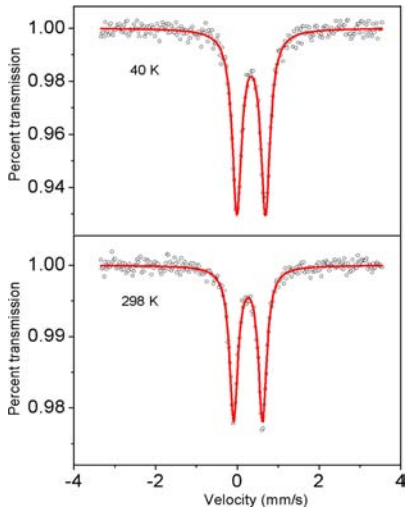

Figure 4. Zero field Mössbauer spectra of *cis*-$\mathbf{1}^{4+}$ at 40 K (top) and 298 K (bottom). The solid line represents a best fit.

Magnetic Measurements. Magnetic susceptibility measurements of *cis*/*trans*-$\mathbf{1}^{4+}$ were performed at 2−300 K, respectively (Figure 5). The temperature dependence of the

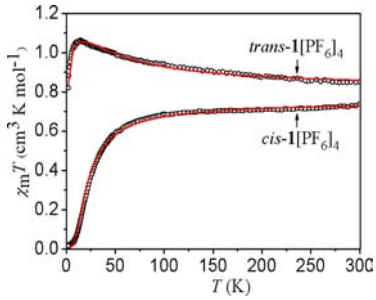

Figure 5. χ_mT vs T in an applied field of 1 kOe for *cis*-$\mathbf{1}^{4+}$ (squares) and *trans*-$\mathbf{1}^{4+}$ (circles). The red solid lines represent the best fit to experimental data with a dinuclear model.

χ_mT product (where χ_m is the molar magnetic susceptibility and T the temperature in Kelvin) of polycrystalline samples of *cis*- and *trans*-$\mathbf{1}^{4+}$ is plotted against T in Figure 5. For *cis*-$\mathbf{1}^{4+}$, χ_mT is equal to 0.74 cm^3 K mol^{-1} at room temperature, which is close to the spin-only value (0.75 cm^3 K mol^{-1}) expected for the two low-spin Fe(III) ions. As the temperature decreases, χ_mT remains quasi-constant down to 100 K and then decreases more and more rapidly, indicative of antiferromagnetic interactions between the Fe^{III}_2 pairs. When paramagnetic impurities α are considered, the experimental data can be closely fitted to eq 1 from modified Bleaney−Bowers equation (N, g, k, and β are the Avogadro number, the Zeeman factor, the Boltzmann constant, and the Bohr magneton, respectively).[13] The fit gives J = −13.6 cm^{-1}, g = 2.00, α = 0.01, and an agreement factor $R = 1 \times 10^{-4}$ ($R = \sum_i(\chi T_i^{calc} - \chi T_i^{exp})/(\chi T_i^{exp})^2$). The temperature dependence of $1/\chi_m$ (where χ_m is the molar magnetic susceptibility) in the temperature range

dx.doi.org/10.1021/ic401604q | Inorg. Chem. 2013, 52, 11343−11350

45−300 K follows Curie−Weiss behavior with C = 0.75 cm^3 K mol^{-1} and θ = −12.08 K (C is Curie constant and θ Weiss constant), further suggesting an antiferromagnetic interaction for *cis*-**1**$^{4+}$ (Supporting Information, Figure S10).

$$\chi_m T = (1 - a)\frac{2Ng^2\beta^2}{k} \times \frac{1}{3 + e^{-2J/kT}} + a\frac{2Ng^2\beta^2}{3k} \quad S(S + 1) \tag{1}$$

$$\chi_m T = \frac{2Ng^2\beta^2}{k} \times \frac{e^{-D/3kT}}{e^{2D/3kT} + 2e^{-D/3kT} + e^{-2J/kT}} \tag{2}$$

For *trans*-**1**$^{4+}$, $\chi_m T$ at 300 K is 0.85 cm^3 K mol^{-1}. As the temperature is lowered, $\chi_m T$ increases steadily and reaches a maximum of 1.06 cm^3 K mol^{-1} (corresponding to a low-lying state with S = 1 and g = 2.06) at 14.9 K and then decreases sharply due to zero-field splitting and/or intermolecular interactions, being consistent with ferromagnetically coupled Fe^{III}_2 pairs. The magnetic properties could be analyzed by using the spin Hamiltonian including zero field splitting D in equation $H = -2JS_A \cdot S_B + S_A \cdot D \cdot S_B$. The best fit to the data using eq 2 gives J = 11.6 cm^{-1}, g = 2.09, D = 0.43, and an agreement factor $R = 6 \times 10^{-5}$.[14] Such a large positive J value in *trans*-**1**$^{4+}$ obviously indicates a strong ferromagnetic coupling between the two distant Fe(III) ions. The temperature dependence of $1/\chi_m$ in the temperature range 2−300 K follows Curie−Weiss behavior with C = 0.85 cm^3 K mol^{-1} and θ = 5.13 K (Supporting Information, Figure S11). The Weiss constant value also suggests a ferromagnetic interaction for complex *trans*-**1**$^{4+}$.

Theoretical Calculations. To explain the origin of the magnetic properties of Prussian Blue, Mayoh and Day speculated as early as in 1976 that it should be resulted from the partial electron delocalization from the low-spin Fe^{II} onto the neighboring high-spin Fe^{III} ions.[15] Recently, Achim and coworkers experimentally observed for the first time the spin density at the LS Fe^{II} site induced by the paramagnetic Cr^{III} ions, which resulted in the weak ferromagnetic coupling between the axial Cr^{III} centers mediated by the equatorial diamagnetic Fe^{II} ions in $[Fe(tmphen)_2]_3[Cr(CN)_6]_2$.[6b] The study of the spin density distribution is important and useful in understanding the mechanism of the magnetic coupling between paramagnetic centers in polynuclear compounds.[16] To explore the mechanism of the magnetic coupling and how the magnetic interaction is affected by the configuration of the central bridging metalloligand, DFT calculations were performed for *cis*/*trans*-**1**$^{4+}$ compounds (see the Supporting Information). Since the value of J is very sensitive to the geometry and a small variation in the geometry can lead to obvious changes of the calculated coupling constant, the experimental geometries (including the anions) are employed in the calculations in order to compare the theoretical results with the experimental values. Our results indicate that for *cis*-**1**$^{4+}$, the antiferromagnetic interaction is preferred, while ferromagnetic coupling becomes favorable for *trans*-**1**$^{4+}$. According to the total energies of different spin states, the predicted J values for *cis*- and *trans*-**1**$^{4+}$ are −14.8 and 23.4 cm^{-1}, respectively, which are close to the experimental results. The calculated spin densities of two complexes (Supporting Information, Table S1) agree with a spin delocalization mechanism through the π orbitals of CN bridges. This is evidenced by the spin density distribution (Figure 6), which reveals that the spin densities of the two compounds are

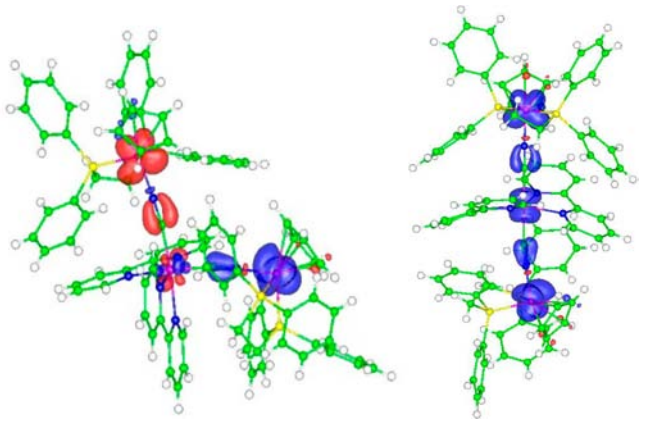

Figure 6. The calculated spin density distributions for the ground singlet spin state of *cis*-**1**$^{4+}$ (left) and the ground triplet spin states of *trans*-**1**$^{4+}$ (right). Blue and red contours represent positive and negative spin densities, respectively. Only one unit is shown and the isodensity surface corresponds to a value of ±0.02e Å^{-3}. In the case of *cis*-**1**$^{4+}$ compound, the xz plane is defined as a plane containing Ru and two Fe atoms.

primarily concentrated on the Fe atoms, and the corresponding magnitude of each Fe is about 0.81e (Supporting Information, Table S1). Some spin densities at two cyanido bridges are also observed, and additionally for the ground triplet spin state of *trans*-**1**$^{4+}$ the spin density at the Ru atom is also obvious (0.26e). As shown in Figure 6, it is quite clear that the π orbitals of the CN bridges, which are made up of p_x/p_y-type orbitals of the N and C atoms, overlap with the d_π orbitals (namely d_{xz}/d_{yz}) of the Fe and Ru atoms. Since the spin densities of cyanido bridges have the same sign as that of the neighboring Fe atoms, it can be regarded that the long distance magnetic exchange interactions between the two distant Fe(III) centers of both *cis*-**1**$^{4+}$ and *trans*-**1**$^{4+}$ are due to the spin-delocalization mechanism.

Now let us discuss how the configuration of the complex affects the magnetic coupling between the two Fe^{III} ions. For clarity, we first focus on *trans*-**1**$^{4+}$ with a linear structure. The analyses of the partial density of states (PDOS) of five 3d orbitals of the metal atoms (Supporting Information, Figure S12) demonstrate that for both the singlet and triplet spin states of *trans*-**1**$^{4+}$, unpaired electrons are mainly associated with the d_π orbitals of the Fe and Ru atoms. However, it is worth noting that the planes of π orbitals of two cyanido bridges are not coplanar, because the noncoplanar arrangement of the two terminal Cp(dppe)Fe fragments can reduce the steric hindrance between the ligands around the Ru and Fe ions. The twist angle (ϕ) between the planes of the two π orbitals is defined in Figure 7a, and the corresponding value for *trans*-**1**$^{4+}$ is estimated to be about 121°. This also implies that the central Ru^{II} ion must provide different d_π orbitals, d_{xz} and d_{yz} to interact with two π orbitals of neighboring CN bridges, respectively.

The variation of the magnetic coupling for *trans*-**1**$^{4+}$ as a function of the ϕ value has been investigated by constructing a model complex, in which only one unit of *trans*-**1**$^{4+}$ is involved in the calculations, and one phenyl group of dppe of a Fe atom is replaced by a methyl group to avoid a too small distance between bpy and dppe ligands at some ϕ values (Supporting Information, Figure S13). It must be mentioned that, due to the simplification of the ligand and omitting the solvent molecules, the calculated J value of this model system may differ from the

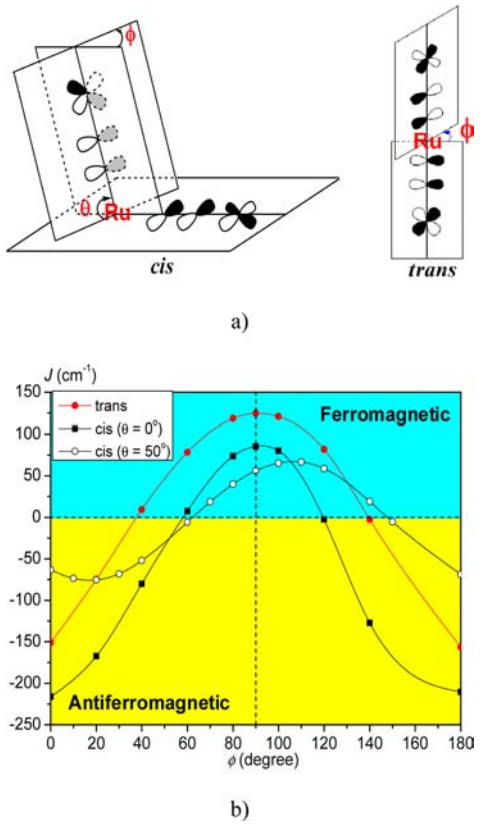

Figure 7. (a) Schematic illustration of the twist angle (ϕ) between the planes of the π orbitals of two CN bridges in *cis*- and *trans*-$\mathbf{1}^{4+}$, as well as the tilted angle (θ) in the *cis* compound. (b) Variation of the coupling constant (J) as a function of ϕ of model *cis*- and *trans*-$\mathbf{1}^{4+}$ compounds. In part a, the d_π orbitals of the Ru atom are not shown, but they can be deduced from the planes of the π orbitals of two neighboring CN bridges.

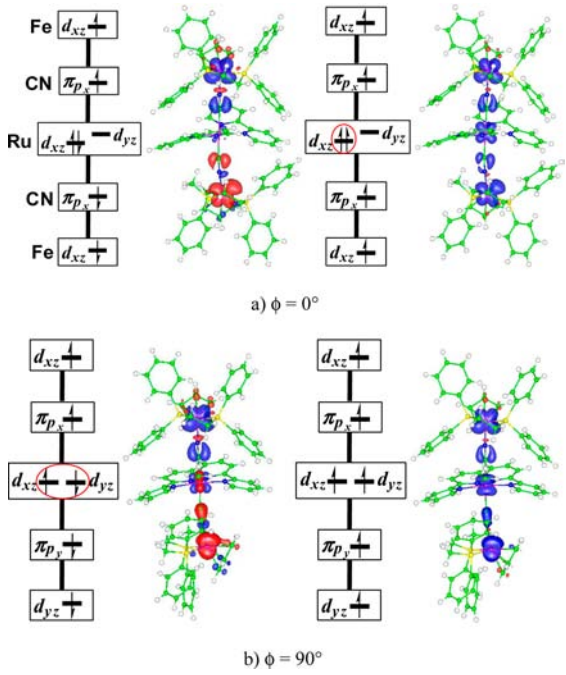

Figure 8. Schematic illustration of the magnetic coupling mechanisms and the spin density distributions of the singlet (left) and triple spin states (right) of the model *trans*-complex with (a) $\phi = 0°$ and (b) $\phi = 90°$.

result obtained by using the experimental crystal structure with the same ϕ value. The variation of the J value is presented in Figure 7b. As can be seen, when the value of ϕ varies from 0° to 180°, the ground state first switches from the singlet spin state to the triple spin state, and then back from the triple spin state to the singlet spin state, which indicates that the magnetic coupling of the system is sensitive to the ϕ value. Especially, it is predicted that the strongest intramolecular antiferromagnetic and ferromagnetic couplings are achieved when the orientations of the π orbitals of the two CN bridges are coplanar ($\phi = 0°$ and 180°) and orthogonal ($\phi = 90°$), respectively. The above different magnetic couplings can be well explained by considering the electron occupations and energy splitting of the two d_π orbitals of the central Ru atom. As illustrated in Figure 8a, for $\phi = 0°$, the Ru^{II} ion only offers a d_{xz} orbital to overlap with the π orbitals of the two cyanido bridges that are made up of the p_x orbitals of the C and N atoms, while d_{yz} of Ru^{II} is not involved in the interaction with the π orbitals. Consequently, the d_{xz} and d_{yz} orbitals of Ru^{II} are non-degenerate, and the d_{xz} orbital becomes doubly occupied (Figure 8a). According to the assignment of two electrons, it is obvious that the triplet state with the same spin orientation of two d_{xz} electrons (circled in Figure 8a) is unreasonable. Therefore, the antiferromagnetic coupling is favored at $\phi = 0°$, and as verified by the calculated spin density distribution (Figure 8a), the spin density at the Ru^{II} ion can be negligible. On the other hand, in the case of $\phi = 90°$, both d_{xz} and d_{yz} orbitals of Ru^{II} interact with π orbitals of two cyanido bridges, which are composed of the p_x and p_y orbitals, respectively. Care must be taken that now the d_{xz} and d_{yz} orbitals are degenerate due to the orthogonal arrangement of the two d_π orbitals (Figure 8b). So following Hund's rule, now the triplet state that the unpaired d_{xz} and d_{yz} electrons that have the same spin will be stabilized, compared to the corresponding singlet state (circled in Figure 8b). Furthermore, since the reversion of the magnetic coupling for the *trans* structure occurs at about $\phi = 38°$ and 139° (Figure 7b), it seems that the ferromagnetic coupling can be obtained in a wider range of ϕ ($38° < \phi < 139°$) than the antiferromagnetic coupling ($\phi < 38°$ or $\phi > 139°$). At the experimental ϕ value (121°) of *trans*-$\mathbf{1}^{4+}$, a ground triplet spin state with ferromagnetic coupling between two Fe^{III} ions is also predicted for the above model system.

In the *cis*-$\mathbf{1}^{4+}$ compound, the relative arrangement of the two π orbitals is more complicated than that in the *trans* compound, and in addition to the twist angle, the tilted angle (denoted by symbol θ in Figure 7a) also has a significant influence on the magnetic coupling. For a special case with $\theta = 0°$, the change of J with the ϕ value for the corresponding model complex is given in Figure 7b, which shows similar variation as observed in the *trans* compound. For instance, the strongest antiferromagnetic and ferromagnetic couplings are also predicted when the π orbitals of the two CN bridges are coplanar and orthogonal, respectively. Further analyses indicate that the magnetic interactions in this special *cis* complex have the same origins as those found in the *trans* compound (Supporting Information, Figure S14). When the value of θ is not zero, for example, at the experimental value of about 50°, the corresponding model *cis* complex will exhibit different magnetic behavior. From the curve shown in Figure 7b, a distinct feature is that the positions of the strongest antiferromagnetic and ferromagnetic couplings are shifted to $\phi = 20°$ and 105°, respectively. This is directly related to the different π-topology

dx.doi.org/10.1021/ic401604q | *Inorg. Chem.* 2013, 52, 11343−11350

where the plane of one CN-π orbital is inclined to that of the other one (Figure 7a). Therefore, unlike the *trans* configuration and the *cis* compound with $\theta = 0°$, the calculated spin density distributions (Supporting Information, Figure S15) reveal that there are some residual spin densities at the Ru^{II} ion for the ground singlet spin state with $\phi = 20°$, and for the ground triplet spin state with $\phi = 105°$, the spin density at the Ru^{II} ion is distorted obviously to simultaneously match two CN-π orbitals on both sides. Moreover, if the experimental ϕ value of the *cis*-$\mathbf{1}^{4+}$ compound (about 45.5°) is employed, a ground singlet state is preferred (Figure 7b) and in agreement with the *cis*-$\mathbf{1}^{4+}$ complex exhibits the antiferromagnetic coupling between two Fe^{III} ions.

CONCLUSIONS

In summary, the first example of the *cis*-/*trans*-isomer with multistates, *cis*-/*trans*-[Cp(dppe)Fe(μ-CN)Ru(bpy)$_2$(μ-CN)-Fe(dppe)Cp][PF_6]$_2$ (*cis*-/*trans*-**1**[PF_6]$_2$) and their two-electron-oxidation products, [Cp(dppe)Fe(μ-CN)Ru(bpy)$_2$(μ-CN)Fe(dppe)Cp][PF_6]$_4$ (*cis*-/*trans*-**1**[PF_6]$_4$), have been synthesized and structurally characterized. The magnetic measurements and analyses for *cis*/*trans*-$\mathbf{1}^{4+}$ have shown that the two distant Fe^{III} ions in both complexes exhibit similar strong magnetic couplings across a bridging diamagnetic cyanido-metal. As a unique example, however, *cis*-$\mathbf{1}^{4+}$ is antiferromagnetic and *trans*-$\mathbf{1}^{4+}$ is ferromagnetic, which are also confirmed by DFT calculations. According to the calculated spin density distributions, the spin-delocalization mechanism should be responsible for the magnetic coupling between the two distant paramagnetic Fe(III) centers in both *cis*- and *trans*-$\mathbf{1}^{4+}$. Most importantly, these investigations have shown that the type (antiferromagnetic or ferromagnetic) and strength (J) of the magnetic interactions in such compounds can be controlled by the *cis or trans* configuration of the diamagnetic cyanido-metal bridge. Furthermore, it must be mentioned that the interesting geometric variations of the magnetic interactions observed in the present work (especially ϕ angle dependence) are directly related to the low symmetry of the two interacting magnetic centers. To obtain more of an understanding on the magnetism−structure relationship of complexes with diamagnetic cyanido-metal linker, further works to design and synthesize more such complexes with different configurations are in progress.

EXPERIMENTAL SECTION

Materials and Methods. All manipulations are performed under a nitrogen atmosphere with the use of standard Schlenk techniques unless otherwise stated. Dichloromethane and acetonitrile were dried by distilling over calcium hydride under a nitrogen atmosphere. Methanol was dried by distilling over magnesium. The complexes *cis*-[Ru(bpy)$_2$(CN)$_2$][17] (bpy = 2,2′-bipyridine) and *trans*-[Ru(bpy)$_2$(CN)$_2$][18] Cp(dppe)Fe($NCCH_3$)Br[19] (dppe = bis-(diphenylphosphino)ethane) were prepared according to literature procedures. All other reagents were available commercially and used without further purification. Chromatography was on silica gel (100−200 mesh). Elemental analyses (C, H, N) were carried out on Vario MICRO elemental analyzer. Electrospray ion mass spectra (ESI−MS) were performed on a DECAX-30000 LCQ Deca XP Ion Trap Mass Spectrometer using acetonitrile as mobile phases. Infrared (IR) spectra were recorded on a Perkin-Elmer Spectrum One spectrophotometer with KBr pellets. UV−vis−NIR absorption spectra were measured on a Perkin−Elmer Lambda 900 UV−vis−NIR spectrophotometer. ^{31}P NMR spectra were recorded using an AVANCE III NMR spectrometer and are referenced to external 85% H_3PO_4 (0.0 ppm). Magnetic susceptibilities on crystalline samples (22.43 mg for *cis*-**1**[PF_6]$_4$, 24.44 mg for *trans*-**1**[PF_6]$_4$) were measured with a Quantum Design MPMS-XL SQUID susceptometer under an applied magnetic field of 1 kOe in the 2−300 K range. Diamagnetic corrections were made using Pascal's constants.

*Synthesis of cis-[Ru(bpy)$_2$(CN)$_2$][CpFe(dppe)]$_2$[PF_6]$_2$, cis-**1**[PF_6]$_2$.* To a 20 mL methanol solution of *cis*-[Ru(bpy)$_2$(CN)$_2$] (70 mg, 0.150 mmol) was added 2 equiv of Cp(dppe)Fe($NCCH_3$)Br (193.0 mg, 0.30 mmol) at room temperature. The reaction mixture was heated to 50 °C and stirred under a nitrogen atmosphere for 5 h, resulting in a color change from red brown to black brown; then NH_4PF_6 (50.0 mg) was added to the above reaction solution. The mixture was stirred for another 5 h and was concentrated under reduced pressure. The residue was loaded onto a silica gel column and eluted with CH_3OH/CH_2Cl_2 (1:100−1:50, v/v) to yield 140 mg of dark red brown powder (52%). The black brown crystal was obtained by slowly diffusing diethylether to the dichloromethane solution of *cis*-**1**[PF_6]$_2$. Data for *cis*-**1**[PF_6]$_2$, Anal. Cacld for $RuFe_2C_{84}H_{74}N_6P_6F_{12}$: C, 56.23; H, 4.16; N, 4.68. Found: C, 56.79; H, 4.30; N, 4.72. ^{31}P NMR (400 MHz, CD_3OD): δ 97.84 (Fe(II)-P), −144.17 (PF_6). IR (KBr, cm^{-1}): 2086 (s) (C≡N). UV−vis−NIR (CH_3CN) λ_{max}, nm (ε, M^{-1} cm^{-1}): 362 (7253), 480 (5620). ESI-MS m/z: 1645.4 [**1**(PF_6)$_2$-PF_6]$^+$.

*Synthesis of cis-[Ru(bpy)$_2$(CN)$_2$][CpFe(dppe)]$_2$[PF_6]$_4$, cis-**1**[PF_6]$_4$.* To an 8 mL dichloromethane solution of *cis*-**1**[PF_6]$_2$ (57.0 mg, 0.032 mmol) freshly prepared in methanol was added 2 equiv of $(Cp)_2FePF_6$ (21.0 mg, 0.064 mmol) at room temperature. The solution changed immediately from dark red brown to dark green. The green deposition was collected by filtration after 3 h. Layering diethylether onto the acetonitrile solution of deposition afforded dark green crystals (35 mg, 0.0168 mmol, 52%). Data for *cis*-**1**[PF_6]$_4$, Anal. Cacld for $RuFe_2C_{84}H_{74}N_6P_8F_{24}\cdot 2H_2O$: C, 47.59; H, 3.71; N, 3.96. Found: C, 47.50; H, 3.65; N, 4.03. IR (KBr, cm^{-1}): 2059 (m) (C≡N), 2021 (s) (C≡N). UV−vis−NIR (CH_3CN) λ_{max}, nm (ε, M^{-1} cm^{-1}): 391 (8363), 722 (8238). ESI-MS m/z: 1939.1 [**1**(PF_6)$_4$-PF_6]$^+$.

*Synthesis of trans-[Ru(bpy)$_2$(CN)$_2$][CpFe(dppe)]$_2$[PF_6]$_2$, trans-**1**[PF_6]$_2$.* To a 15 mL methanol solution of *trans*-[Ru(bpy)$_2$(CN)$_2$] (54 mg, 0.116 mmol) was added 2 equiv of Cp(dppe)Fe($NCCH_3$)Br (150 mg, 0.232 mmol) at room temperature. The reaction mixture was heated to 65 °C and stirred under a nitrogen atmosphere for 6 h, resulting in a red purple solution. NH_4PF_6 (45.0 mg) was then added to the above reaction solution. An amount of red purple precipitate appeared immediately and was collected (180 mg, 86%). Deep brown crystals of *trans*-**1**[PF_6]$_2$ suitable for X-ray diffraction can be obtained by slowly diffusing diethylether to the dichloromethane solution of red purple precipitate at room temperature. Data for *trans*-**1**[PF_6]$_2$, Anal. Cacld for $RuFe_2C_{84}H_{74}N_6P_6F_{12}$: C, 56.23; H, 4.16; N, 4.68. Found: C, 55.61; H, 4.64; N, 4.24. ^{31}P NMR (400 MHz, CD_3OD): δ 99.66 (Fe(II)-P), −144.63 (PF_6). IR (KBr, cm^{-1}): 2099 (s) (C≡N). UV−vis (CH_3CN) λ_{max}, nm (ε, $M^{-1}c$ m^{-1}): 376 (11851), 528 (7727). ESI-MS m/z: 1648.8 [**1**(PF_6)$_2$-PF_6]$^+$.

*Synthesis of trans-[Ru(bpy)$_2$(CN)$_2$][CpFe(dppe)]$_2$[PF_6]$_4$, trans-**1**[PF_6]$_4$.* To a 8 mL dichloromethane solution of *trans*-**1**[PF_6]$_2$ (60.0 mg, 0.033 mmol) freshly prepared in methanol was added 2 equiv of $(Cp)_2FePF_6$ (22.1 mg, 0.067 mmol) at room temperature. The solution changed immediately from purple brown to dark brown. The reaction mixture was stirred for 1 h and concentrated to 2 mL under reduced pressure, and then 50 mL of diethylether was added to precipitate the gray brown product in a 92% yield. Layering diethylether onto the acetonitrile solution of deposition afforded dark brown crystals (40 mg, 0.0192 mmol, 58%). Data for *trans*-**1**[PF_6]$_4$, Anal. Cacld for $RuFe_2C_{84}H_{74}N_6P_8F_{24}$: C, 48.41; H, 3.58; N, 4.03. Found: C, 47.82; H, 3.84; N, 4.04. IR (KBr, cm^{-1}): 2041 (m) (C≡N). UV−vis−NIR (CH_3CN), λ_{max}, nm (ε, $M^{-1}cm^{-1}$): 418 (13689), 783 (12938). ESI-MS m/z: 1939.0 [**1**(PF_6)$_4$-PF_6]$^+$.

X-Ray Structure Determination. The crystals of *cis*-**1**[PF_6]$_2$, *cis*-**1**[PF_6]$_4$, *trans*-**1**[PF_6]$_2$, and *trans*-**1**[PF_6]$_4$ were sealed in capillaries with mother liquors and measured on a Mercury-CCD diffractometer equipped with graphite-monochromatic Mo Kα (λ = 0.71073 Å) radiation by using an ω scan mode at 293.2 K. The structure was solved by direct methods and the heavy atoms and refined on F^2 by

full-matrix least-squares techniques using the SHELX97 program package.[20] The large solvent accessible voids in the structures of *cis*-**1**$[PF_6]_n$ (n = 2, 4) arise from the loss of crystallization solvent molecules. All non-hydrogen atoms were refined anisotropically, and the hydrogen atoms were generated geometrically with isotropic thermal displacements.

Electrochemistry. Electrochemical measurements were performed in argon using *V*3-Studio in acetonitrile solutions containing 0.1 M (nBu$_4$N)PF$_6$ as a supporting electrolyte at a scan rate of 100 mV s^{-1}. Glassy graphite and platinum were used as working and counter electrodes, respectively, and the potentials were measured against a Ag/AgCl reference electrode. Ferrocene was added as an internal standard on the experiment.

Mössbauer Spectra. The ^{57}Fe Mössbauer spectra were obtained by using a conventional constant acceleration type spectrometer in transmission geometry. The gamma-ray source is 25 mCi ^{57}Co in a Rh matrix, and the driver velocity was calibrated using an α-Fe foil. All of the spectra were fitted with the hyperfine field distribution using a slightly modified version of the Hesse and Rübartsch method using the MossWinn program.[21]

Theoretical Calculations. First-principles calculations based on density functional theory were carried out utilizing the Vienna *ab initio* simulation package (VASP)[22] and the projected augmented wave (PAW).[23] The generalized gradient approximation Perdew–Burke-Ernzerhof (PBE) exchange-correlation functional was employed.[24] The kinetic energy cutoff for the plane-wave expansion was set to 500 eV, and the effects of spin polarization were involved. The calculations of the magnetic exchange coupling constants (J) of *cis*/*trans*-**1**$[PF_6]_4$ compounds were performed using experimental geometries with compositions of $C_{336}H_{320}N_{24}O_{12}F_{96}P_{32}Fe_8Ru_4$ (for *cis*) and $C_{184}H_{180}N_{20}O_4F_{48}P_{16}Fe_4Ru_2$ (for *trans*), respectively. Considering the large size of the cell and the weak interactions between adjacent units, only the Γ point was chosen for Brillouin zone integration. During investigation of the magnetic coupling mechanisms (Figure 7 in the text) of *cis*/*trans*-**1**$[PF_6]_4$ compounds, the corresponding model complexes were constructed, in which only one unit of *cis*/*trans*-**1**$[PF_6]_4$ was involved in the calculations (placed in a 30 × 30 × 30 Å cubic box). In addition, to avoid too small of a distance between bpy and dppe ligands at some twist angles, one phenyl group of the dppe ligand of an Fe atom was replaced by a methyl group (for example, circled in Figure S13).

■ ASSOCIATED CONTENT

Supporting Information

X-ray crystallographic data in CIF format: CCDC-900621 (*cis*-**1**$[PF_6]_2$), 900620 (*cis*-**1**$[PF_6]_4$), 900622 (*trans*-**1**$[PF_6]_2$), and 900623 (*trans*-**1**$[PF_6]_4$). Cyclic voltammogram for *trans*-**1**$[PF_6]_2$, IR spectra, crystallographic data and molecular structures for *cis*-/*trans*-**1**$[PF_6]_n$ (n = 2, 4), Mössbauer spectra for *trans*-$\mathbf{1}^{4+}$ at 40 and 298 K, $1/\chi_m$ vs. T for *cis*-$\mathbf{1}^{4+}$ and *trans*-$\mathbf{1}^{4+}$, theoretical calculations in detail. This material is available free of charge via the Internet at http://pubs.acs.org.

■ AUTHOR INFORMATION

Corresponding Authors

*E-mail: zhangyf@fzu.edu.cn.
*E-mail: tsheng@fjirsm.ac.cn.

Notes

The authors declare no competing financial interest.

■ ACKNOWLEDGMENTS

This work was supported by grants from the 973 Program (2012CB821702), the National Science Foundation of China (21073192, 21173223, 21233009, 21373048, and 21073035), and the Science Foundation of CAS (KJCX2-YW-H20).

■ REFERENCES

(1) (a) Holmes, S. M.; Girolami, G. S. *J. Am. Chem. Soc.* **1999**, *121*, 5593. (b) Sato, O.; Iyoda, T.; Fujishima, A.; Hashimoto, K. *Science* **1996**, *272*, 704. (c) Ferlay, S.; Mallah, T.; Ouahes, R.; Veillet, P.; Verdaguer, M. *Nature* **1995**, *378*, 701. (d) Entley, W. R.; Girolami, G. S. *Science* **1995**, *268*, 397. (e) Hoshino, N.; Iijima, F.; Newton, G. N.; Yoshida, N.; Shiga, T.; Nojiri, H.; Nakao, A.; Kumai, R.; Murakami, Y.; Oshio, H. *Nature Chem.* **2012**, *4*, 921–926.

(2) See the recent reviews: (a) Wang, S.; Ding, X.-H.; Li, Y.-H.; Huang, W. *Coord. Chem. Rev.* **2012**, *256*, 439. (b) Wang, X. Y.; Avendano, C.; Dunbar, K. R. *Chem. Soc. Rev.* **2011**, *40*, 3213. (c) Newton, G. N.; Nihei, M.; Oshio, H. *Eur. J. Inorg. Chem.* **2011**, 3031. (d) Atanasov, M.; Comba, P.; Hausberg, S.; Martin, B. *Coord. Chem. Rev.* **2009**, *253*, 2306. (e) Tanase, S.; Reedijk, J. *Coord. Chem. Rev.* **2006**, *250*, 2501. (f) Przychodzen, P.; Korzeniak, T.; Podgajny, R.; Sieklucka, B. *Coord. Chem. Rev.* **2006**, *250*, 2234. (g) Sieklucka, B.; Podgajny, R.; Przychodzen, P.; Korzeniak, T. *Coord. Chem. Rev.* **2005**, *249*, 2203. (h) Lescouezec, R.; Toma, L. M.; Vaissermann, J.; Verdaguer, M.; Delgado, F. S.; Ruiz-Perez, C.; Lloret, F.; Julve, M. *Coord. Chem. Rev.* **2005**, *249*, 2691. (i) Beltran, L. M. C.; Long, J. R. *Acc. Chem. Res.* **2005**, *38*, 325. (j) Miller, J. S.; Manson, J. L. *Acc. Chem. Res.* **2001**, *34*, 563. (k) Ohba, M.; Okawa, H. *Coord. Chem. Rev.* **2000**, *198*, 313. (l) Verdaguer, M.; Bleuzen, A.; Marvaud, V.; Vaissermann, J.; Seuleiman, M.; Desplanches, C.; Scuiller, A.; Train, C.; Garde, R.; Gelly, G.; Lomenech, C.; Rosenman, I.; Veillet, P.; Cartier, C.; Villain, F. *Coord. Chem. Rev.* **1999**, *192*, 1023. (m) Dunbar, K. R.; Heintz, R. A. *Prog. Inorg. Chem.* **1997**, *45*, 283.

(3) Shatruk, M.; Avendano, C.; Dunbar, K. R. *Prog. Inorg. Chem.* **2009**, *56*, 155.

(4) (a) Buser, H. J.; Schwarzenbach, D.; Petter, W.; Ludi, A. *Inorg. Chem.* **1977**, *16*, 2704. (b) Buser, H. J.; Ludi, A. *J. Chem.Soc., Chem. Comm.* **1972**, 1299.

(5) Ito, A.; Suenaga, M.; Ono, K. *J. Chem. Phys.* **1968**, *48*, 3597.

(6) (a) Halbauer, K.; Spielberg, E. T.; Sterzik, A.; Plass, W.; Imhof, W. *Inorg. Chim. Acta* **2010**, *363*, 1013. (b) Shatruk, M.; Dragulescu-Andrasi, A.; Chambers, K. E.; Stoian, S. A.; Bominaar, E. L.; Achim, C.; Dunbar, K. R. *J. Am. Chem. Soc.* **2007**, *129*, 6104. (c) Halbauer, K.; Leibeling, G.; Imhof, W. *Z. Anorg. Allg. Chem.* **2006**, *632*, 264. (d) Yuan, A. H.; Lu, L. D.; Shen, X. P.; Chen, L. Z.; Yu, K. B. *Trans. Met. Chem.* **2003**, *28*, 163. (e) Smekal, Z.; Travnicek, Z.; Mrozinski, J.; Marek, J. *Inorg. Chem. Commun.* **2003**, *6*, 1395. (f) Panja, A.; Shaikh, N.; Vojtisek, P.; Gao, S.; Banerjee, P. *New J. Chem.* **2002**, *26*, 1025. (g) Kou, H. Z.; Si, S. F.; Gao, S.; Liao, D. Z.; Jiang, Z. H.; Yan, S. P.; Fan, Y. G.; Wang, G. L. *Eur. J. Inorg. Chem.* **2002**, 699. (h) Rogez, G.; Marvilliers, A.; Riviere, E.; Audiere, J. P.; Lloret, F.; Varret, F.; Goujon, A.; Mendenez, N.; Girerd, J. J.; Mallah, T. *Angew. Chem., Int. Ed.* **2000**, *39*, 2885. (I) Ma, X.; Hu S, M.; Tan, C. H.; Wen, Y. H.; Zhu, Q. L.; Shen, C. J.; Sheng, T. L.; Wu, X. T. *Dalton Trans.* **2012**, *41*, 12163.

(7) Freedman, D. E.; Jenkins, D. M.; Iavarone, A. T.; Long, J. R. *J. Am. Chem. Soc.* **2008**, *130*, 2884.

(8) (a) Bignozzi, C. A.; Argazzi, R.; Schoonover, J. R.; Gordon, K. C.; Dyer, R. B.; Scandola, F. *Inorg. Chem.* **1992**, *31*, 5260. (b) Sheng, T.; Vahrenkamp, H. *Eur. J. Inorg. Chem.* **2004**, 1198. (c) Watzky, M. A.; Endicott, J. F.; Song, X. Q.; Lei, Y. B.; Macatangay, A. *Inorg. Chem.* **1996**, *35*, 3463.

(9) Kettle, S. F. A.; Diana, E.; Marchese, E. M. C.; Boccaleri, E.; Croce, G.; Sheng, T. L.; Stanghellini, P. L. *Eur. J. Inorg. Chem.* **2010**, 3920.

(10) (a) Bignozzi, C. A.; Roffia, S.; Scandola, F. *J. Am. Chem. Soc.* **1985**, *107*, 1644. (b) Albores, P.; Rossi, M. B.; Baraldo, L. M.; Slep, L. D. *Inorg. Chem.* **2006**, *45*, 10595.

(11) Hush, N. S. *Prog. Inorg. Chem.* **1967**, *8*, 391.

(12) Sato, M.; Hayashi, Y.; Kumakura, S.; Shimizu, N.; Katada, M.; Kawata, S. *Organometallics* **1996**, *15*, 721.

(13) Paul, F.; Bondon, A.; da Costa, G.; Malvolti, F.; Sinbandhit, S.; Cador, O.; Costuas, K.; Toupet, L.; Boillot, M. L. *Inorg. Chem.* **2009**, *48*, 10608.

(14) Kahn, O. *Molecular Magnetism*; VCH: New York, 1993.

(15) Mayoh, B.; Day, P. *J. Chem. Soc., Dalton Trans.* **1976**, 1483.

(16) (a) Ruiz, E.; Rodriguez-Fortea, A.; Alvarez, S.; Verdaguer, M. *Chem.—Eur. J.* **2005**, *11*, 2135. (b) Ruiz, E.; Cirera, J.; Alvarez, S. *Coord. Chem. Rev.* **2005**, *249*, 2649.
(17) (a) Bignozzi, C. A.; Roffia, S.; Chiorboli, C.; Davila, J.; Indelli, M. T.; Scandola, F. *Inorg. Chem.* **1989**, *28*, 4350. (b) Coe, B. J.; Meyer, T. J.; White, P. S. *Inorg. Chem.* **1993**, *32*, 4012.
(18) (a) Sprintschnik, G.; Sprintschnik, H. W.; Kirsch, P. P.; Whitten, D. G. *J. Am. Chem. Soc.* **1977**, *99*, 4947. (b) Durham, B.; Wilson, S. R.; Hodgson, D. J.; Meyer, T. J. *J. Am. Chem. Soc.* **1980**, *102*, 600.
(19) Treichel, P. M.; Molzahn, D. C. *Synth. React. Inorg. Met.-Org. Chem.* **1979**, *9*, 21.
(20) Sheldrick, G. M. *Acta. Crystallogr., Sect. A* **2008**, *64*, 112.
(21) (a) Hesse, J.; Rübartsch, A. *J. Phys. E: Sci. Instrum.* **1974**, *7*, 526. (b) Klencsár, Z.; Kuzmann, E.; Vértes, A. *J. Radioanal. Nucl. Chem.* **1996**, *210*, 105.
(22) (a) Kresse, G.; Hafner, J. *Phys. Rev. B* **1993**, *47*, 558. (b) Kresse, G.; Furthmuller, J. *Phys. Rev. B* **1996**, *54*, 11169.
(23) Blöchl, P. E. *Phys. Rev. B* **1994**, *50*, 17953.
(24) Perdew, J. P.; Burke, K.; Ernzerhof, M. *Phys. Rev. Lett.* **1996**, *77*, 3865.